ISSN 1063-7761, Journal of Experimental and Theoretical Physics, 2021, Vol. 133, No. 3, pp. 374–381. © Pleiades Publishing, Inc., 2021.
Russian Text © The Author(s), 2021, published in Zhurnal Eksperimental'noi i Teoreticheskoi Fiziki, 2021, Vol. 160, No. 3, pp. 443–452.

ELECTRONIC PROPERTIES OF SOLID

Electronic Properties of NiO at Ultrahigh Pressure

S. G. Ovchinnikov[a,*] and T. M. Ovchinnikova[b]

[a] *Kirensky Institute of Physics, Federal Research Center "Krasnoyarsk Scientific Center, Siberian Branch, Russian Academy of Sciences," Krasnoyarsk, 660036 Russia*

[b] *Sukachev Institute of Forest, Federal Research Center "Krasnoyarsk Scientific Center, Siberian Branch, Russian Academy of Sciences," Krasnoyarsk, 660036 Russia*

**e-mail: sgo@iph.krasn.ru*

Received March 16, 2021; revised March 16, 2021; accepted May 27, 2021

Abstract—The effect of the high pressure on the electronic properties of NiO is studied within the multielectron approach. The low energy physics is described by the effective Hubbard model based on Ni *d*-electrons and O *p*-electrons in three charge sectors of the Hilbert space: neutral states (configurations $d^8 + d^9\underline{L} + d^{10}\underline{L}^2$), electron removal states (configurations $d^7 + d^8\underline{L} + d^9\underline{L}^2$), and electron addition states ($d^9 + d^{10}\underline{L}$) with $\underline{L}$ denotes a ligand hole. Due to a high spin (HS)-low spin (LS) crossover in the electron removal states at pressure P_S determined by a competition of the intraatomic Hund exchange interaction and increasing with pressure crystal field 10Dq, the effective Hubbard parameter U_{eff} and the insulator gap E_g depend on pressure. We find weak increasing of E_g for $P < P_S$ and weak decreasing E_g for $P > P_S$. The Mott-Hubbard transition pressure is estimated to be in the interval 450–650 GPa.

DOI: 10.1134/S106377612109003X

1. INTRODUCTION

Strongly correlated electronic systems (SCES) include many novel materials such as Mott insulators, high-T_c superconductors, manganites with colossal magnetoresistance, multiferroics, heavy fermion materials, etc. Strong local Coulomb interactions result in the specific properties of SCES. NiO is one of the most important SCES compounds. Firstly, it was considered by Mott [1] to demonstrate a deviation from a single electron band theory and to explain the origin of the Mott insulators. It is expected that under high external pressure a broadening of the bandwidth will result in the insulator-metal transition (IMT) with the closing of the insulator gap E_g and delocalization of 3*d* electrons [2] and the collapse of magnetic moments [3]. In many other 3*d* metal monoxides the IMT and magnetic collapse are known above 70 GPa in FeO [3, 4], between 80 and 100 GPa in MnO [5, 6], and above 120 GPa in CoO [7, 8]. The NiO has so far been found to be stable up to 147 GPa [9], no magnetic collapse has been found by nuclear forward scattering of synchrotron radiation up to 280 GPa [10]. Pressure-dependent insulator gap E_g from the change of the optical absorption spectra and the IMT from transport measurements at 240 GPa have been found in [11]. According to the authors [11], the measured IMT in NiO is most probably due to minor charge carriers from impurities and not reflects intrinsic physics.

Density functional theory (DFT) nowadays is quite successful in condensed matter physics to treat itinerant electrons in periodic crystal lattices [12]. Nevertheless, for SCES its simplest versions like the LDA and GGA usually failed [13]. Localized electrons can be better treated in the cluster approaches with more adequate accounts for strong Coulomb interactions. For NiO, a cluster model was proposed in [14, 15]. In this approach a $(NiO_6)^{10-}$ cluster is treated as a separable unit and its electronic structure is described by configuration interaction. Although translational symmetry is ignored, local interactions can be treated explicitly. The most important interactions included are the *d*–*d* Coulomb interactions and the O 2*p*–Ni 3*d* hybridization. This is done by consideration of the two-hole configurations contributing to the ground state (d^8, $d^9\underline{L}$, and $d^{10}\underline{L}^2$), the one-hole states contributing to the electron-affinity (BIS) spectrum (d^9 and $d^{10}\underline{L}$), and the three-hole states contributing to the ionization (XPS) spectrum (d^7, $d^8\underline{L}$, $d^9\underline{L}^2$, and $d^{10}\underline{L}^3$). Holes are defined relative to filled 3*d* and ligand (O2*p*) states and $\underline{L}$ denotes a ligand hole. Within the cluster approach, it was concluded that NiO is not a Mott–Hubbard insulator [16]. A general classification of two competing insulator states, the Mott-Hubbard insulator, and the charge-transfer insulator, has been proposed by Zaanen, Sawatzky, and Allen [17]. It appears that NiO can be placed in the intermediate regime of the Zaanen, Sawatzky, and Allen phase diagram. A recent analysis of the X-ray experimental data and the

NiO electronic structure within the cluster approach can be found in [18].

To treat SCES within the Hubbard model several different numerical approaches, such as quantum Monte Carlo (QMC) [19–23], cluster perturbation theory (CPT) [24, 25], variational cluster approximation (VCA) [26], dynamical mean-field theory (DMFT) [27], its cluster (CDMFT) [28, 29] extensions, and other techniques designed for dealing with strongly correlated systems [30–34], see the recent review [35]. To introduce effects of strong correlations in the density functional theory several hybrid schemes have been invented, the LDA+DMFT with a local self-energy [36–39] and its cellular extensions [29, 40–42].

To combine the advantages of the band and the cluster approaches to SCES a multielectron generalized tight-binding (GTB) method was suggested [43]. In this method, the ideas of the Hubbard model treatment in the regime of strong correlations [44] are developed for the multiband p–d model that allows considering the different SCES like cuprates, manganites, cobaltates etc. The tight-binding model parameters can be calculated from ab initio within the hybrid LDA+GTB approach [45, 46]. The low energy limit within the GTB is described by the effective Hubbard model with the parameter $U_{\text{eff}} = E_0(n+1) + E_0(n-1) - 2E_0(n)$ [17], where $E_0(n)$ is the ground term of the MeO_6 cluster with n electrons, for NiO $n = 8$. Similar to the cluster approaches [14, 15] the ground term $E_0(n)$ is formed by a mixture of d^n, $d^{n+1}\underline{L}$, $d^{n+2}\underline{L}^2$ configurations. The intercluster electron hopping can be written in terms of the multielectron Hubbard X-operators constructed within $n-1$, n, and $n+1$ cluster eigenstates. It allows going beyond the cluster model and calculating the electronic structure of a lattice within this effective Hubbard model. At high pressure, different d^n configurations may undergo a spin-crossover from HS to LS state, such crossover results in the pressure-dependent $U_{\text{eff}}(P)$ [47, 48]. Recently we have considered the effect of high pressure on the electronic structure of CoO [49].

In this paper, we consider the high-pressure effect on the electronic structure and properties of NiO. The peculiarity of NiO is the stability of the neutral d^8 and electron addition d^9 states and the HS to LS crossover in the electron removal configuration d^7. This crossover results in a kink in the $U_{\text{eff}}(P)$ dependence. Our theory contains two pressure-dependent parameters, the pressure derivatives of the crystal field and the pressure derivatives of the bandwidth. The first one has been found by [50] from the pressure-dependent optical d–d excitations. The second one we have estimated from the pressure-dependent Néel temperature [51]. Then we can extrapolate the insulator gap to zero to estimate that the Mott-Hubbard transition and magnetic collapse in NiO may be expected in the interval 450–650 GPa.

The rest of the paper is organized as follows. The main ideas of the multielectron generalized tight-binding (GTB) approach and its relation to the exact Lehmann representation are discussed in Ch. 2. The effect of spin crossover in the first electron removal states on the pressure dependence of $U_{\text{eff}}(P)$ is described in Ch. 3. Estimation of the electron bandwidth increment α_w from the experimental data for the Néel temperature $T_N(P)$ is discussed in Ch. 4. Chapter 5 contains the analysis of the insulator gap E_g pressure dependences below and above the spin crossover. The estimation of critical pressure of the IMT transition within two approaches is also given in Ch. 5. The linear extrapolation of the bandwidth results in the $P_{\text{IMT}} = 900$ GPa, the more realistic approach using the Birch–Murnaghan equation of states gives the P_{IMT} in the interval 450–650 GPa. Discussion of results is given in Ch. 6.

2. MAIN IDEAS OF THE MULTIELECTRON GENERALIZED TIGHT-BINDING (GTB) APPROACH

To clarify a notion of an electron in strongly correlated materials where convenient theory based on renormalized free electrons is inadequate we start with the exact Lehmann representation for the single-electron Green function [52], which at $T = 0$ can be written as

$$G_\sigma(k,\omega) = \sum_m \left(\frac{A_m(k,\omega)}{\omega - \Omega_m^+} + \frac{B_m(k,\omega)}{\omega - \Omega_m^-} \right).$$

The poles of this function are given by a set of single-particle excitations (quasiparticles, QP) with the energies

$$\Omega_m^+ = E_m(N+1) - E_0(N) - \mu,$$
$$\Omega_m^- = E_0(N) - E_m(N-1) - \mu,$$

and spectral weight

$$A_m(k,\omega) = |\langle 0, N|a_{k\sigma}|m, N+1\rangle|^2,$$
$$B_m(k,\omega) = |\langle m, N-1|a_{k\sigma}|0, N\rangle|^2.$$

Here $|m, N\rangle$ is the mth eigenstate of the system with N electrons,

$$H|m, N\rangle = E_m|m, N\rangle$$

At finite temperature the Lehmann representation for the Green function can be written in the following way

$$G_\sigma^R(k,\omega) = \sum_{mn} W_n \frac{A_{mn}(k,\omega)}{\omega - \Omega_{mn}^+ + i0}(1 + e^{-\Omega_{mn}^+/T}).$$

Here, the QP as the excitation between the initial state n and final one m has the energy

$$\Omega^{+}_{mn} = E_m(N+1) - E_n(N) - \mu,$$

the statistical weight of a state $|n\rangle$ is determined by the Gibbs distribution with the thermodynamic potential Ω:

$$W_n = \exp\{(\Omega - E_n + \mu N)/T\}.$$

At non-zero temperature both the ground state $|0, N\rangle$ and the excited states $|n, N\rangle$ are partially occupied. Thus a QP is numerated by a pair of indexes (m, n). It is a single electron excitation in the multielectron system due to addition of one electron to the initial N-electron state $|n, N\rangle$ with formation the final $(N+1)$-electron state $|m, N+1\rangle$. The electron addition energy is $\Omega^{+}_{mn} = E_m(N+1) - E_n(N) - \mu$, while the electron removal energy is $\Omega^{-}_{mn} = E_m(N) - E_n(N-1) - \mu$. In practical calculations the Lehmann representation is useless because the multielectron eigenstates $|m, N\rangle$ for crystal are not known.

The GTB method is the cluster perturbation realization of the multielectron ideas of the Lehmann representation. In this approach, the total Hamiltonian is rewritten as a sum of all intracluster terms, H_f, $H_0 = \Sigma H_f$, and the sum of all intercluster terms, H_{fg}, $H_{\rm int} = \Sigma H_{fg}$. The intracluster term H_f includes all d electrons and nearest oxygen p orbitals that are orthogonalized to form molecular orbitals centered at site f (see [45, 46] for details) and all local interactions of p and d electrons. The numerical exact diagonalization of the local part provides the exact multielectron eigenenergies and eigenstates, $H_f|m\rangle = E_m|m\rangle$. Similar to the conventional Hubbard model, we introduce the Hubbard operators $X_f^{m,n} = |m\rangle\langle n|$, determined by a set of exact intracluster eigenstates. Then the local part of the total Hamiltonian becomes diagonal $H_f = \Sigma_m E_m X_f^{m,m}$ and describes the energy of the multielectron terms $|m\rangle$ in different configurations. The Hilbert space of the exact eigenstates for the NiO_6 cluster is shown schematically in Fig. 1. Here the occupied at $T = 0$ d^8 ground term with $S = 1$ is marked by a cross, and the excited d^8 singlet is empty. The electron removal terms of the d^7 configuration are the HS with $S = 3/2$ and LS excited $S = 1/2$ terms for the low pressure (Fig. 1a), which become inverted above spin crossover, see Eq. (4) below (Fig. 1b). For electron addition d^9 states we show only the ground term with $S = 1/2$.

The next step in the GTB is to include effects of the intercluster hopping and interactions that are treated by a perturbation theory. Analysis of the diagram expansion within the Hubbard operator diagram technique [53] results in the exact generalized Dyson equation [54] for the fermionic quasiparticles with electrical charge e and spin 1/2. Thus electron is a linear combination of excitations between different multielectron terms similar to the Lehmann representation. They were called the Hubbard electrons in the GTB approach to emphasize the difference with a free electron.

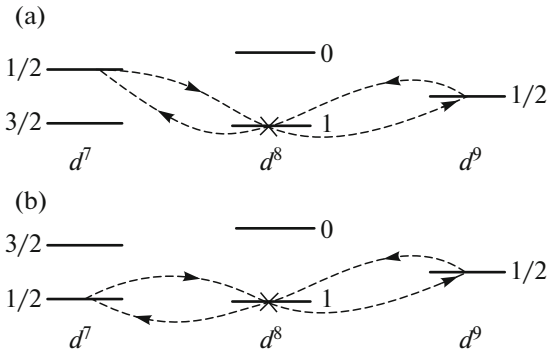

Fig. 1. A scheme of the multielectron terms of the NiO_6 cluster for 3 sectors of the Hilbert space with electron numbers 8 (charge-neutral) states, electron removal (7 electrons) configuration, and electron addition (9 electrons) configuration. For each term its spin value is shown, the occupied at $T = 0$ ground d^8 term is marked by a cross. Dotted lines show virtual electron-hole pair excitations forming the 180° antiferromagnetic superexchange interaction of the next nearest magnetic cations. The upper part (a) corresponds to a small pressure $P < P_S$, and part (b) is for $P > P_S$.

3. LOW ENERGY EFFECTIVE HUBBARD MODEL

It is well known that strong correlations split the one-electron band in the Hubbard model into the lower and upper Hubbard subbands (LHB and UHB, respectively). In the conventional Hubbard model with an orbitally nondegenerate band of width $2W$ and an intraatomic Coulomb Hubbard parameter U, the band gap in the limit of strong electron correlations ($U \gg W$), $E_g = U - W$, decreases with the growth of pressure P due to the band broadening resulting from the interatomic distance decrease, $W(P) = W(0) + \alpha_W P$. This leads to the Mott–Hubbard insulator-metal transition in the case of a half-filled band when the band half-width attains the critical value $W_c = aU$ ($a \sim 1$) [1, 44]. The Hubbard parameter U is of an intraatomic nature and is assumed to be pressure-independent. The situation becomes different in multiorbital analogs of the Hubbard model, which can be used to describe NiO. For such models, the initial Hubbard concepts should be supplemented by taking into account various multielectron d^n terms and anionic sp states. In the low-energy range, the effective Hamiltonian of such multiband p–d model within the GTB approach can be written in the form of the effective Hubbard model, in which the d^0, d^1, and d^2 atomic terms of the single-band Hubbard model are replaced by local multielectron d^7, d^8, and d^9 terms [17, 55]. Here each d^n term is just a notation meaning the

hybridized $d^n + d^{n+1}\underline{L} + d^{n+2}\underline{L}^2$ as in the cluster approaches. In the atomic limit ($W = 0$), the analogs of LHB and UHB correspond to energies $\Omega_v = E_0(d^8) - E_0(d^7)$ (a valence band) and $\Omega_c = E_0(d^9) - E_0(d^8)$, (a conductivity band) respectively. It is assumed that the average number of electrons is $\langle n_e \rangle = 8$. Then, the gap between UHB and LHB is determined by the effective Hubbard parameter [17]

$$U_{\text{eff}} = \Omega_c - \Omega_v = E_0(9) + E_0(7) - 2E_0(8). \quad (1)$$

Owing to the competition between the intraatomic Hund's exchange coupling J_H and the cubic component of the crystal field $10Dq$, each d^n term ($n = 4$–7) can have either HS or LS ground states [56]. The HS–LS spin-crossover can occur due to the growth of the crystal field with pressure, which can also be approximated by the linear dependence $10Dq(P) = 10Dq(0) + \alpha\Delta P$ [57]. As a result, the spin crossover changes $U_{\text{eff}}(d^n)$, suggesting a relationship with the Mott–Hubbard transition. The effect of the spin-crossover on the electron correlation parameter turns out to be not universal; for d^5 ions, U_{eff} is suppressed, whereas for d^6 ions, U_{eff} increases due to the spin crossover [47, 48, 58], for d^7 ion in CoO the U_{eff} does not change at the spin crossover [49].

For NiO only the first electron removal state can reveal a spin-crossover between the two terms:

(a) the high-spin (HS) term with spin $S = 3/2$ and energy

$$E_{\text{HS}}(d^7) = E_C(d^7) - 8Dq - 11J_H; \quad (2)$$

(b) the low-spin (LS) term with spin $S = 1/2$ and energy

$$E_{\text{LS}}(d^7) = E_C(d^7) - 18Dq - 9J_H. \quad (3)$$

Here, $E_C(d^7)$ is the spin-independent part of the Coulomb interaction for seven electrons at a $(NiO_6)^{9-}$ cluster. From these formulas, we can see that for a free ion at zero crystal field, the high-spin state is more favorable in energy, but with an increase in the crystal field, the energy of the low-spin state decreases faster, and both energies become equal at $10Dq = 2J_H$. This condition corresponds to the pressure

$$P_S = (2J_H - 10Dq(0))/\alpha_\Delta. \quad (4)$$

For d^8 and d^9 configurations the ground state energy may be written as

$$E(d^8) = E_C(d^8) - 12Dq - 13J_H, \quad (5)$$

$$E(d^9) = E_C(d^9) - 6Dq - 16J_H. \quad (6)$$

Finally we can write down the $U_{\text{eff}}(P)$ below and above crossover pressure P_S in the following way

$$U_{\text{eff}} = \begin{cases} U(8) + 10Dq - J_H, & P < P_S \\ U(8) + J_H, & P > P_S. \end{cases} \quad (7)$$

Here $U(8) = E_C(d^9) + E_C(d^7) - 2E_C(d^8)$ is pressure-independent contribution. The pressure-dependent insulator gap is given by

$$E_g(P) = \begin{cases} U(8) - J_H + \Delta_0 - W(0) + (\alpha_\Delta - \alpha_W)P, & P < P_S \\ U(8) + J_H - W(0) - \alpha_W P, & P > P_S. \end{cases} \quad (8)$$

Here we denoted $10Dq\ (P = 0) = \Delta_0$. One can see from Eq. (8) that increasing crystal field at small pressure below spin-crossover tends to the insulator gap growth, while the increasing bandwidth tends to the gap decreasing for all pressures. Thus the HS–LS crossover for compounds with d^8 ionic states competes with a tendency to the insulator-metal transition (IMT) under the pressure growth. Depending on the relations between two baric derivatives α_Δ and α_W, the gap may change the initial growth to the decreasing with further pressure increase or monotonically decrease with pressure. Anyhow, in both cases, the gap will have a kink at the spin-crossover pressure P_S in the unoccupied d^7 configuration.

4. DISCUSSION OF MODEL PARAMETERS

Some parameters are known from the literature. For example, the crystal field at ambient pressure $\Delta_0 = 0.08Ry = 1.08$ eV is found from optical absorption spectra [59, 60], its baric derivative $\alpha_\Delta = 7.28$ meV/GPa taken from pressure-dependent optical spectra [50]. The bandwidth $W(0)$ and Coulomb parameters U and J_H have been estimated from the analysis [16] of the experimental data. Additional fitting of these parameters using the pressure-dependent optical absorption spectra of NiO has been provided in [11] and yields the following best fit

$$U(8) = U = 5.45 \text{ eV},$$
$$J_H = 0.75 \text{ eV}, \quad W(0) = 1.8 \text{ eV}.$$

With these parameters, the spin crossover pressure $P_S = 57.7$ GPa is very close to the kink in the gap E_g at 55 GPa measured in [11]. The only still unknown parameter is the baric derivative of the bandwidth W, below we discuss how we use the Néel temperature $T_N(P)$ baric dependence [51], $dT_N/dP = 7.33$ K/GPa, to estimate this parameter. In the Anderson theory [61] for NiO, the 180° antiferromagnetic superexchange interaction of the next nearest magnetic cations is known to be $J = 2t^2/U_{\text{eff}}$. Here t is the interatomic cation-anion-cation electron hopping parameter that determines the bandwidth $W(0) = 6t_0$. With $W(0) = 1.8$ eV one gets $t_0 = 0.3$ eV. For NiO the nearest neighbors 90° exchange is negligibly small and we will neglect it. The parameter $U_{\text{eff}} = U + J_H$ in the denominator of the effective Heisenberg exchange in the case of NiO is determined by virtual electron-hole pair creation and annihilation. These excitations involve the

LS electron removal term (see Fig. 1), at $P = 0$ the ground d^7 term has $S = 3/2$, but the AFM exchange coupling occurs via $S = 1/2$ LS d^7 term for all pressures [62], so for $P = 0$ in the mean-field approximation to the effective Heisenberg model with the exchange interaction J, $S = 1$ and number of second neighbors $z_2 = 6$ the Néel temperature is given by

$$T_N(0) = S(S+1)Jz_2/3 = 8t_0^2/(U + J_H). \quad (9)$$

Its baric derivative is equal to

$$dT_N/dP = \frac{16t_0}{U + J_H}\alpha_t,$$

where α_t determines the hopping parameter increase under pressure, $t(P) = t_0 + \alpha_t P$. With the given above parameters U, J_H, t_0 and the experimental value $dT_N/dP = 7.33$ K/GPa measured in [39] below 30 GPa, we obtained $\alpha_t = 9.47$ K/GPa $= 0.815$ meV/GPa. The baric dependence of the bandwidth $\alpha_W = 6\alpha_t = 4.89$ meV/GPa.

Now we are ready to discuss the insulator gap (8) at ambient pressure and its pressure dependence. At zero pressure $E_g(0) = 3.98$ eV. Due to the larger crystal field baric derivative $\alpha_\Delta = 7.28$ meV/GPa vs. $\alpha_W = 6\alpha_t = 4.89$ meV/GPa the gap increases up to the spin crossover pressure P_S (Fig. 2). At the crossover point $E_g(P_S) = 4.12$ eV. The baric dependence of the gap 2.39 meV/GPa can be compared with experimental value 2.78 ± 0.3 meV/GPa from Fig. S5 in the supplement to the paper [11].

Above spin-crossover the gap is decreasing with the increment $-\alpha_W = -4.89$ meV/GPa, which can be compared with the experimental value -5 ± 0.3 meV/GPa [11]. Assuming the same linear trend, we extrapolate the gap given by Eq. (8) to zero to estimate the IMT pressure $P_{IMT} = 900$ GPa. It should be mentioned that linear extrapolation of the crystal field and the electronic bandwidth pressure dependences, which is valid at small pressures below 240 GPa (linear dependence of the gap has been measured in [11] up to this pressure), is questionable at higher pressures. That is why below we present the other estimation of the bandwidth and the IMT pressure using the Birch–Murnaghan equation of states. It is known that the interatomic hopping parameter for d electrons depends on the interatomic distance as $t \sim r^{-5}$ [63]. We write this relation as a function of volume

$$t(P) = t_0(V/V_0)^{-5/3}, \quad (10)$$

where t_0 and V_0 are the hopping parameter and volume at ambient pressure. The volume and the pressure are related via the Birch-Murnaghan equation of states. Denote $u = V/V_0$, we write this equation as

$$P = \frac{3}{2}B_0[u^{-7/3} - u^{-5/3}] \times\left\{1 - \frac{3}{4}(4 - B')(u^{-2/3} - 1)\right\}. \quad (11)$$

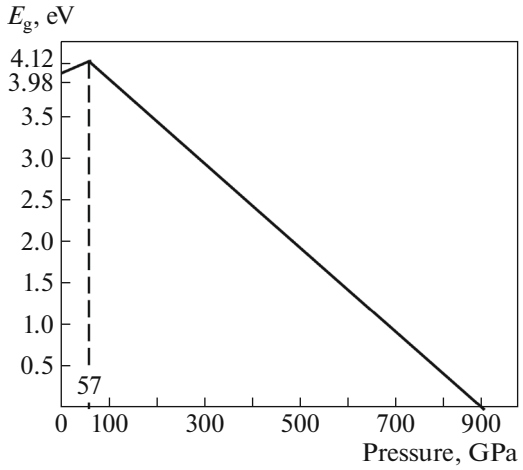

Fig. 2. The insulator gap in NiO and its pressure dependence.

We introduce a new variable

$$x(P) = (V/V_0)^{-5/3}.$$

Then the equation for the critical pressure of the insulator-metal transition looks like

$$E_g(P_{IMT}) = U + J_H - W_0 x(P_{IMT}) = 0. \quad (12)$$

The critical pressure can be found from the condition

$$x(P_{IMT}) = (U + J_H)/W_0. \quad (13)$$

We emphasize that this condition does not contain linear extrapolation and is valid for all pressure values. For the set of parameters $U = 5.45$ eV, $J_H = 0.75$ eV, $W_0 = 1.8$ eV found in [11], the critical value is given by

$$x(P_{IMT}) = 3.44. \quad (14)$$

For this value of x one can find the critical volume at the IMT, $V/V_0 = 0.47$ and the critical pressure $P/B_0 = 2.34$ (Fig. 3). For the bulk modulus from [50] $B_0 = 197$ GPa and $B' = 3.4$ we obtain $P_{IMT} = 461$ GPa.

This solution depends on the bulk modulus values that are different in the literature. In Table 1 we present a set of data chosen from the literature. When several pairs B_0 and B' were available from the same authors, we take the data measured at small pressure to avoid the non-hydrostatic effects. From this table it is clear that the expected value of the P_{IMT} is 450–650 GPa, and the value 900 GPa obtained within the linear extrapolation is too overestimated.

5. DISCUSSION OF RESULTS

In this paper, we take the empirical values of the model parameters, mainly found from the pressure dependences of optical absorption spectra [11] and the baric dependence of the Néel temperature. Now we

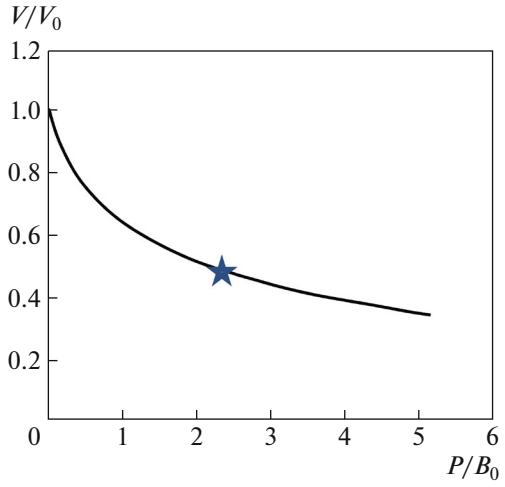

Fig. 3. The volume dependence on the dimensionless pressure from the Birch–Murnaghan equation. The critical point of the insulator-metal transition is shown by a star.

can compare the ambient pressure gap $E_g(0) = 3.98$ eV with the values 4.3 eV obtained by XPS and BIS measurements [16] and 4 eV by XAS and XES measurements [14, 66, 67]. There are a lot of theoretical papers with different DFT-based approaches to calculate electronic parameters and spectra of NiO [3, 14, 68–84] as well as experimental studies [9–11, 16, 50, 70, 85–90]. The main conclusion from these papers is the importance of strong electron correlations that is the central idea of our paper. We want also to mention the DFT paper [84] with hybrid potential B3LYP, which gives a reasonable value for zero pressure gap $E_g(0) =$ 4.2 eV and the IMT pressure 2.4 TPa and magnetic collapse at 3.7 TPa. With the other choice of the calculation scheme, the PWGGA, the same authors obtained $E_g(0) = 1.3$ eV and the IMT pressure 700 GPa. Our approach is too oversimplified to treat fine details of NiO electronic spectra. Nevertheless, it allows us to understand the origin of the kink in the insulator gap dependence on pressure found previously from optical spectra study [11].

Table 1. The NiO bulk modulus from different experimental groups and the calculated values of the critical pressure for the insulator-metal transition

Authors	B_0, GPa	B'	P_{IMT}, GPa
Gavrilyuk et al. [50]	197	3.4	461
Potapkin et al. [10]	170	4.35	552
Eto et al. [9]	192	4.0	634
Huang [65]	187	4.0	617
Liu et al. [64]	189	4.0	624

As concerning the high-pressure experiments, the kink at 55 GPa [11] is very well reproduced by our calculations. Assuming linear dependence of the crystal field and electronic bandwidth we have obtained both the kink position as well as slopes of the gap pressure dependence below and above the kink in very good agreement to experimental data [11]. The origin of the kink is related to the spin crossover in the electron-removal d^7 subspace of the total Gilbert space. We want to emphasize that all d^7 terms are not occupied in the stoichiometric samples. These states are involved in the formation of the electronic structure only virtually. The kink in the insulator gap is the demonstration of the multielectron effects. The extrapolation of the linear bandwidth pressure dependence results in the IMT at pressure 900 GPa, which is too large a value for the linear extrapolation. We have developed the alternative approach of the estimation of the bandwidth at large pressures using the know expression of the hopping parameter on the interatomic distance and the Birch-Murnaghan equation. One can see from Fig. 3 that the linear dependence of the crystal volume on the pressure can be considered below 100 GPa. At higher pressures, the nonlinear dependence of $V(P)$ results in much smaller values of the IMT pressure. From Table 1 these values are within 450–650 GPa interval.

This high value agrees with the stability of the magnetic state in NiO at least up to 280 GPa [10]. Previously the insulator-metal transition in NiO was found in [11] at pressure 240 GPa. It is accompanied by the change of slope of the resistivity vs. pressure that is typical for the insulator-metal transition, and the activation energy from resistivity measurements drops to zero. Nevertheless, the absolute value of the activation energy below transition is about 0.15 eV, that is why the authors [11] themselves consider this effect as metallization of some minor charge carriers related to sample defects.

In summary, NiO is the most stable Mott insulator among other 3*d*-monoxides. We have found that the insulator gap dependence on pressure is characterized by the kink resulting from the HS–LS crossover in the unoccupied d^7 configuration. These states contribute to the formation of the insulator gap due to the effects of strong correlations. Our analysis shows the IMT and magnetic collapse are expected at very high pressure within 450–650 GPa intervals.

ACKNOWLEDGMENTS

We are thankful to Dr. Alexander Gavriliuk and Dr. Leonid Dubrovinsky for stimulating discussions. We thank the Russian Science Foundation for the financial support under the project no. 18-12-00022.

REFERENCES

1. N. F. Mott, *Metal-Insulator Transitions*, 2nd ed. (Taylor and Francis, London, 1990).
2. I. G. Austin and N. F. Mott, Science (Washington, DC, U. S.) **168**, 71 (1970).
3. R. E. Cohen, I. I. Mazin, and D.G. Isaak, Science (Washington, DC, U. S.) **275**, 654 (1997).
4. J. Kunes, A. V. Lukoyanov, V. I. Anisimov, et al., Nat. Mater. **7**, 198 (2008).
5. J.-P. Rueff, A. Mattila, J. Badro, et al., J. Phys.: Condens. Matter **17**, S717 (2005).
6. C. S. Yoo, B. Maddox, J.-H. P. Klepeis, et al., Phys. Rev. Lett. **94**, 115502 (2005).
7. Q. Guo, H. K. Mao, J. Hu, et al., J. Phys.: Condens. Matter **14**, 11369 (2002).
8. T. Atou, M. Kawasaki, and S. Nakajima, Jpn. J. Appl. Phys. **43**, L1281 (2004).
9. T. Eto, S. Endo, M. Imai, et al., Phys. Rev. B **61**, 14984 (2000).
10. V. Potapkin, L. Dubrovinsky, I. Sergueev, et al., Phys. Rev. B **93**, 201110 (2016).
11. A. G. Gavriliuk, I. A. Trojan, and V. V. Struzhkin, Phys. Rev. Lett. **109**, 086402 (2012).
12. W. E. Pickett, Rev. Mod. Phys. **61**, 433 (1989).
13. T. C. Leung, C. T. Chan, and B. N. Harmon, Phys. Rev. B **44**, 2923 (1991).
14. A. Fujimori and F. Minami, Phys. Rev. B **29**, 5225 (1984).
15. G. v. d. Laan, C. Westra, C. Haas, et al., Phys. Rev. B **23**, 4369 (1981).
16. G. A. Sawatzky and J. W. Allen, Phys. Rev. Lett. **53**, 2339 (1984).
17. J. Zaanen, G. A. Sawatzky, and J. W. Allen, Phys. Rev. Lett. **55**, 418 (1985).
18. C.-Y. Kuo, T. Haupricht, J. Weinen, et al., Eur. Phys. J. Spec. Top. **226**, 2445 (2017).
19. N. Bulut, D. J. Scalapino, and S. R. White, Phys. Rev. B **50**, 7215 (1994).
20. R. Preuss, W. Hanke, and W. von der Linden, Phys. Rev. Lett. **75**, 1344 (1995).
21. R. Preuss, W. Hanke, C. Gröber, et al., Phys. Rev. Lett. **79**, 1122 (1997).
22. C. Gröber, R. Eder, and W. Hanke, Phys. Rev. B **62**, 4336 (2000).
23. B. Moritz, F. Schmitt, W. Meevasana, et al., New J. Phys. **11**, 093020 (2009).
24. D. Sénéchal, D. Perez, and M. Pioro-Ladrière, Phys. Rev. Lett. **84**, 522 (2000).
25. D. Sénéchal, D. Perez, and D. Plouffe, Phys. Rev. B **66**, 075129 (2002).
26. M. Potthoff, M. Aichhorn, and C. Dahnken, Phys. Rev. Lett. **91**, 206402 (2003).
27. A. Georges, G. Kotliar, W. Krauth, et al., Rev. Mod. Phys. **68**, 13 (1996).
28. M. H. Hettler, M. Mukherjee, M. Jarrell, et al., Phys. Rev. B **61**, 12739 (2000).
29. T. Maier, M. Jarrell, T. Pruschke, et al., Rev. Mod. Phys. **77**, 1027 (2005).
30. R. O. Zaitsev, Sov. Phys. JETP **43**, 574 (1976).
31. N. M. Plakida and V. S. Oudovenko, J. Exp. Theor. Phys. **104**, 230 (2007).
32. A. Avella and F. Mancini, Phys. Rev. B **75**, 134518 (2007).
33. M. M. Korshunov and S. G. Ovchinnikov, Eur. Phys. J. B **57**, 271 (2007).
34. A. Sherman, J. Phys.: Condens. Matter **30**, 195601 (2018).
35. G. Rohringer, H. Hafermann, A. Toschi, et al., Rev. Mod. Phys. **90**, 025003 (2018).
36. V. I. Anisimov, A. I. Poteryaev, M. A. Korotin, et al., J. Phys.: Condens. Matter **9**, 7359 (1997).
37. A. I. Lichtenstein and M. I. Katsnelson, Phys. Rev. B **57**, 6884 (1998).
38. K. Held, I. A. Nekrasov, N. Blumer, et al., Int. J. Mod. Phys. B **15**, 2611 (2001).
39. G. Kotliar, S. Y. Savrasov, K. Haule, et al., Rev. Mod. Phys. **78**, 865 (2006).
40. M. H. Hettler, A. N. Tahvildar-Zadeh, M. Jarrell, et al., Phys. Rev. B **58**, R7475 (1998).
41. G. Kotliar, S. Y. Savrasov, G. Palsson, et al., Phys. Rev. Lett. **87**, 186401 (2001).
42. M. Potthoff, Eur. Phys. J. B **32**, 249 (2003).
43. S. G. Ovchinnikov and I. S. Sandalov, Phys. C (Amsterdam, Neth.) **161**, 607 (1989).
44. J. C. Hubbard, Proc. R. Soc. London, Ser. A **285**, 542 (1965).
45. M. M. Korshunov, V. A. Gavrichkov, S. G. Ovchinnikov, Z. V. Pchelkina, I. A. Nekrasov, M. A. Korotin, and V. I. Anisimov, J. Exp. Theor. Phys. **99**, 559 (2004).
46. M. M. Korshunov, S. G. Ovchinnikov, E. I. Shneyder, et al., Mod. Phys. Lett. B **26**, 1230016 (2012).
47. S. G. Ovchinnikov, J. Exp. Theor. Phys. **107**, 140 (2008).
48. I. S. Lyubutin, S. G. Ovchinnikov, A. G. Gavriliuk, et al., Phys. Rev. B **79**, 085125 (2009).
49. V. A. Gavrichkov, Yu. S. Orlov, T. M. Ovchinnikova, et al., JETP Lett. **112**, 241 (2020).
50. A. G. Gavrilyuk, I. A. Trojan, I. S. Lyubutin, et al., J. Exp. Theor. Phys. **92**, 696 (2001).
51. M. J. Massey, N. H. Chen, J. W. Allen, et al., Phys. Rev. B **42**, 8776 (1990).
52. H. Lehmann, Nuovo Cim. **11**, 342 (1954).
53. R. Zaitsev, Sov. Phys. JETP **68**, 207 (1975).
54. S. Ovchinnikov and V. Val'kov, *Hubbard Operators in the Theory of Strongly Correlated Electrons* (Imperial College Press, London, 2004).
55. S. G. Ovchinnikov, Phys. Usp. **40**, 993 (1997).
56. Y. Tanabe and S. Sugano, J. Phys. Soc. Jpn. **9**, 753 (1954).
57. A. G. Gavrilyuk, I. A. Troyan, S. G. Ovchinnikov, et al., J. Exp. Theor. Phys. **99**, 566 (2004).
58. S. G. Ovchinnikov, J. Exp. Theor. Phys. **116**, 123 (2013).
59. D. R. Stephens and H. G. Drickamer, J. Chem. Phys. **34**, 937 (1961).
60. D. Reinen, Ber. Bunsenges Phys. Chem. **69**, 82 (1965).
61. P. W. Anderson, Phys. Rev. **115**, 2 (1959).

62. V. A. Gavrichkov, S. I. Polukeev, and S. G. Ovchinnikov, Phys. Rev. B **101**, 094409 (2020).
63. W. A. Harrison, *Elementary Electronic Structure* (World Scientific, Singapore, 1999).
64. L. Liu, X. D. Li, J. Liu, et al., J. Appl. Phys. **104**, 113521 (2008).
65. E. Huang, High Press. Res. **13**, 307 (1995).
66. S. Hufner, J. Osterwalder, T. Riesterer, et al., Solid State Commun. **52**, 793 (1984).
67. E. Z. Kurmaev, R. G. Wilks, A. Moewes, et al., Phys. Rev. B **77**, 165127 (2008).
68. B. Brandow, Adv. Phys. **26**, 651 (1977).
69. Z.-X. Shen, R. S. List, D. S. Dessau, et al., Phys. Rev. B **44**, 3604 (1991).
70. J. Kunes, V. I. Anisimov, S. L. Skornyakov, et al., Phys. Rev. Lett. **99**, 156404 (2007).
71. M. R. Norman and A. J. Freeman, Phys. Rev. B **33**, 8896 (1986).
72. D. D. Sarma, J. Solid State Chem. **88**, 45 (1990).
73. G. J. M. Janssen and W. C. Nieuwpoort, Phys. Rev. B **38**, 3449 (1988).
74. Z.-X. Shen, C. K. Shih, O. Jepsen, et al., Phys. Rev. Lett. **64**, 2442 (1990).
75. V. I. Anisimov, I. V. Solovyev, M. A. Korotin, et al., Phys. Rev. B **48**, 16929 (1993).
76. V. I. Anisimov, P. Kuiper, and J. Nordgren, Phys. Rev. B **50**, 8257 (1994).
77. O. Bengone, M. Alouani, P. Blöchl, et al., Phys. Rev. B **62**, 16392 (2000).
78. X. Ren, I. Leonov, G. Keller, et al., Phys. Rev. B **74**, 195114 (2006).
79. C. Rodl, F. Fuchs, J. Furthmuller, et al., Phys. Rev. B **79**, 235114 (2009).
80. H. Jiang, R. I. Gomez-Abal, P. Rinke, et al., Phys. Rev. B **82**, 045108 (2010).
81. P. Thunstrom, I. di Marco, and O. Eriksson, Phys. Rev. Lett. **109**, 186401 (2012).
82. S. Das, J. E. Coulter, and E. Manousakis, Phys. Rev. B **91**, 115105 (2015).
83. S. K. Panda, H. Jiang, and S. Biermann, Phys. Rev. B **96**, 045137 (2017).
84. X.-B. Feng and N. M. Harrison, Phys. Rev. B **69**, 035114 (2004).
85. D. E. Eastman and J. L. Freeouf, Phys. Rev. Lett. **34**, 395 (1975).
86. S. J. Oh, J. W. Allen, I. Lindau, et al., Phys. Rev. B **26**, 4845 (1982).
87. G. van der Laan, J. Zaanen, G. A. Sawatzky, et al., Phys. Rev. B **33**, 4253 (1986).
88. O. Tjernberg, S. Söderholm, U. O. Karlsson, et al., Phys. Rev. B **53**, 10372 (1996).
89. M. Taguchi, M. Matsunami, Y. Ishida, et al., Phys. Rev. Lett. **100**, 206401 (2008).
90. J. Weinen, T. Koethe, C. Chang, et al., J. Electron Spectrosc. Relat. Phenom. **198**, 6 (2015).